PERGAMON

International Journal of Heat and Mass Transfer 44 (2001) 989–998

International Journal of HEAT and MASS TRANSFER

www.elsevier.com/locate/ijhmt

Monte Carlo simulation of a nephelometric experiment

J.G. Marakis *, G. Brenner, F. Durst

Institute of Fluid Mechanics, University of Erlangen-Nuremberg, Cauerstrasse 4, D-91058 Erlangen, Germany

Received 11 November 1999; received in revised form 12 April 2001

Abstract

A Monte Carlo method is applied to simulate the extinction of a laser beam collimated on a suspension of fly-ash particles. The objectives are to evaluate the method by comparing predicted angular distributions of the scattered intensities with measurements available in the literature, to investigate the influence of multiple scattering on these measurements and to estimate the sensitivity of the results on the complex refractive index of the medium. The Lorenz–Mie theory is used to model the radiative properties of the particles. The examined cases showed that their scattering behaviour is sensitive on the imaginary part of their refractive index, for which widely varying values are available in the literature. The proportion of multiple scattering in the total scattered intensity, as received in various angular positions, is calculated. That allows the estimation of angular regions where this proportion is minimised.

Keywords: Laser; Monte Carlo; Scattering

1. Introduction

It is desirable to test general solution methods for radiant heat exchange problems against simple experiments where the independent parameters can be controlled precisely and the dependent quantities can be measured with sufficient accuracy. Motivated by this interest, the present article describes the numerical simulation of the nephelometric experiment reported in [1]. In this experiment a cloud, *nephos*, of fly-ash particles was irradiated by a laser beam and the scattered intensity was measured on a grid of angular positions. There are some reasons that make this experiment attractive for numerical simulation.

The first one is that laser beams are used in many diagnostic techniques. General reviews of this wide field are available in [2–4]. A class of these techniques is based on the extinction of the laser by the participating medium. For this class, a model for the beam propagation is useful as the direct step in an inverse analysis [5]. In other laser-based diagnostics, the extinction of the beam is undesirable. In these cases, the application of a detailed radiative transfer model may help to optimise a particular technique or identify its limitations. Laser Doppler anemometry [6], for example, is based on laser scattering from the particles entrained in a flow. However, multiple scattering may reduce the applicability of this method in flows where the particle phase is dense. It is therefore valuable to identify, using a radiative transfer model, the measuring positions where the ratio of the multiple over the total received scattered intensity is minimised. Such an attempt is reported in Section 3.3.

Another reason for simulating a nephelometric experiment is that a laser is monochromatic radiation. In model validation, this fact allows to avoid the intricacies associated with the wavelength dependence of the radiative transfer equation and its terms. In a similar context, the negligible angular divergence of a laser beam offers an additional advantage for model evaluation because it simplifies the treatment of the angular dependent terms. This is particularly interesting for the methods based on ray-tracing, such as Monte Carlo [7,8], discrete transfer [9,10], discrete direction [11], and other variants [12,13], because it offers the possibility to experimentally verify their elementary building block, which is the single ray.

* Corresponding author. Tel.: +49-9131-85-23007; fax: +49-9131-85-23002.

E-mail address: jmarakis@lstm.uni-erlangen.de (J.G. Marakis).

0017-9310/01/$ - see front matter
PII: S0017-9310(00)00163-0

Nomenclature

C	cross-section
f	particle size distribution
g	asymmetry factor
p	probability density function
Q	scattering or extinction efficiency
q	parameter in Eq. (11)
R	cumulative distribution function
S_1, S_2	complex scattering amplitude functions
t	parameter in Eq. (11)
x	size parameter

Greek symbols

Γ	gamma function
ϑ	polar angle
φ	azimuthal angle

Subscripts

20	mean quadratic diameter
c	conditional
i	incident
LMT	Lorenz–Mie theory
m	marginal
p	most probable (peak) diameter
s	scattering

Superscripts

− (overbar)	psd-averaged

Abbreviations

cdf	cumulative distribution function
pdf	probability density function
psd	particle size distribution

In a scattering environment, tracing of a single ray is still a complex algorithmic entity. Three distinct algorithmic steps can be validated through the numerical simulation of a nephelometric experiment: first, calculation of the radiative properties of a single particle; second, extension of these properties from a single particle to a suspension of particles following a size distribution; and third, transfer of the collimated ray through the particle cloud. Relevant experimental work, on the single and cloud particle levels, is reviewed in [14,15], respectively. For the first algorithmic step, the Lorenz–Mie theory (LMT) is adopted in the present study for calculating the extinction and scattering efficiencies and the phase function of a single particle. The assumptions here are that the particles are spherical and homogeneous. In the second step, the parameters calculated by LMT are extended to the particle cloud through averaging over a particle size distribution (psd). The underlying assumption for this averaging is that either the number density of the particles is low per control volume, or the dimensions of every control volume are small enough to avoid multiple scattering within this volume. This assumption allows the calculation of the cloud properties as a simple summation of the corresponding properties of each particle. The third step is the transfer model. For this step, the simulation of the nephelometric experiment may bring into light the influence that the multiple scattering and the extinction of the scattered intensity may have on the measured angular distribution of the scattered radiation.

Another reason that makes the experiment of Boothroyd et al. [1] attractive for simulation is that these authors examined a cloud of fly-ash particles. Fly-ash is considered a significant contributor to radiative heat transfer in pulverised coal furnaces [16–19]. However, measurements of the wavelength dependent optical properties of fly-ash published by Goodwin and Mitchner [20] showed that the imaginary part of the complex refractive index might had been overestimated in previous studies. These measurements were also discussed in [21,22]. Scattering of fly-ash particles has been investigated using Monte Carlo methods by Gupta et al. [18] and Marakis et al. [23]. Both studies examined furnace-like enclosures with the former work accepting imaginary part of the complex refractive index in the range between 0.5 and 0.005, while the latter adopted the newer measurements of Goodwin and Mitchner. The present study approaches the topic of fly-ash scattering from a more microscopic point of view. The nephelometric experiment is a highly simplified configuration compared with the test cases examined in [18,23]. This fact allows the more detailed accumulation of the information generated by tracing the energy packets, which in turn makes possible the quantification of effects such as multiple scattering or absorption of the scattered light.

The numerical investigations that will be presented in this article are based on a Monte Carlo method. The applications of this method in the field of radiative heat transfer have been recently reviewed by Howell [8], while detailed descriptions can be found in textbooks [7,24,25], or monographs [26–28]. The method is formulated in the next section with the emphasis on derivation of the probability density functions (pdf's) used for sampling the scattering directions. The same section describes the algorithm used for calculating the radiative properties of the particle cloud. In Section 3, Monte Carlo is initially validated against the experimental data of Boothroyd et al. [1]. After that, sensitivity analyses aiming to determine the influence of the optical properties and the multiple scattering on the measurements cited in [1] are presented. The concluding remarks of these analyses are discussed and summarised in the last paragraphs.

2. Formulation

2.1. Description of the Monte Carlo algorithm

The nephelometric experiment of Boothroyd et al. [1] is schematically shown in Fig. 1. A laser beam illuminates a cloud of particles suspended in a cylindrical bed and the scattered light is collected on a grid of angular positions ϑ. The fundamental hypothesis for the Monte Carlo simulation of this experiment is to consider the laser beam as being composed of an amount of discrete energy packets. These packets, as they propagate in the bed, may be scattered towards the direction at angle ϑ (Fig. 1, ray A). The angular distribution of the scattered intensity is numerically recovered by tracing these packets until they reach a distant surface, a virtual detector which stands for the collecting optics, where they are counted. The distance of this detector from the centre of the bed is much bigger than the diameter of the bed and therefore the scattering polar angle, referenced to an absolute system of axes attached to the beam, and the detection angle ϑ are practically the same.

Energy packets propagating at angle ϑ after single scattering, may not be detected since they can be either absorbed (Fig. 1, ray B), or they may undergo a second- or higher-order scattering which will change their propagation direction towards some other angle (Fig. 1, ray D). Except from the packets originating from single scattering, the detector at angle ϑ receives packets which have been multiply scattered from all the other directions towards the examined line of sight (Fig. 1, ray C). Furthermore, it is accepted that the virtual detector counts only the packets coming from first- or higher-order scattering. Thermal emission by the particles, or re-emission of the absorbed laser intensity is considered in the present study as negligible. The former assumption is always valid because of the calibration of the nephelometric instrument, while the latter is valid for the experimental conditions that will be examined in Section 3. Dependent scattering is outside the scope of the present study and therefore is not taken into account.

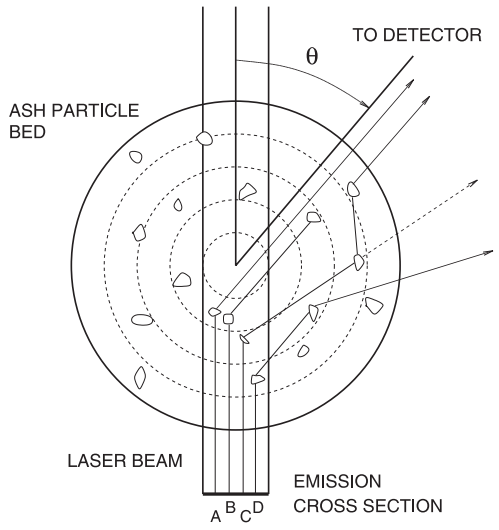

Fig. 1. A schematic of the nephelometric experiment. Ray A: single scattering detected at angle ϑ; rays B and D: extinction after single scattering; ray C: detection of multiple scattering at angle ϑ.

The energy packets are emitted from a cross-section normal to the beam and positioned in an arbitrary small distance outside the bed. The emission points are uniformly distributed on this cross-section. This is done because in the experiment of Boothroyd et al., the beam was initially expanded and then the peripheral part was clipped in order to provide a constant intensity distribution in reference with the beam radius. Furthermore, the polar and azimuth angles of the emission direction are fixed, such that the packets before their first scattering event are always confined within the beam.

Each of the emitted packets carries its own adapted relative system of axes. This system is used to determine the actual position of the energy packet after each propagation step. If propagation is transmission through the medium, then the relative system is simply transferred with the packet. If scattering takes place, the relative system is rotated with angles φ and ϑ, defined in later paragraphs, such that the z-axis always remains coincident with the propagation direction. Transformations between the relative and the absolute system are made using an appropriate rotation matrix. A simple algorithm defines the intersection points between the propagation direction and the surfaces of the control volumes. For each ray, the output of this algorithm is an array containing the lengths travelled within the traced volumes until a boundary is reached. Every time an energy packet is emitted, a random number R_β is calculated. Extinction occurs at the point satisfying the equation

$$\ln R_\beta + \sum_{l=1}^{L-1} s_l \beta_{\lambda,l} + s_L \beta_{\lambda,L} = 0, \tag{1}$$

where $L-1$ are the intersection points, s_l the length travelled inside the lth volume, s_L the distance between the last intersection and the extinction point, and $\beta_{\lambda,l}$ is the monochromatic extinction coefficient of the lth volume.

At the extinction point, the decision whether the energy packet is absorbed or scattered is made by comparing another random variable $R_{\omega,\lambda}$ with the scattering albedo ω_λ of the medium. If $R_{\omega,\lambda}$ is greater than ω_λ, extinction is translated into absorption. In this case, the energy packet is tallied on the counter corresponding to the currently traced volume and the next energy packet is ejected from the emission cross-section. If $R_{\omega,\lambda}$

is less than ω_λ, then extinction is translated into scattering. The energy packets are traced until they reach a coaxial to the bed cylinder which has a radius much bigger than the radius of the bed. This cylinder has a ring which is positioned at the same level as the confined bed and has the same height with it. The ring is subdivided into 360 elements with equal surface, each one representing the collecting optics. If an energy packet hits this ring then, depending on the detection angle ϑ, one of the corresponding 360 counters is increased, otherwise tracing stops and the next energy packet is ejected.

2.2. Sampling of the scattering angles

Scattering is considered as simultaneous absorption and anisotropic re-emission [7]. The functions for sampling the azimuth and polar angles of the after-scattering direction will be systematically derived in the following paragraphs. The reason is that in the general case where scattering is described by a Mueller matrix [29], these angles are not independent and therefore the after-scattering direction is given by a joint probability function. In the special case where radiation is non-polarised, only the S_{11} element of the Mueller matrix is retained, which makes φ and ϑ independent. Non-polarised radiation is experienced in furnaces. This is the reason why the polarisation state of the laser beam used in the nephelometric experiment in [1] was turned to circular, which is an acceptable approximation of non-polarised radiation. The azimuthally independent phase function which is derived by retaining only the S_{11} element was discussed in [30], and it will also be adopted in this study. Nevertheless, the derivation of sampling functions for φ and ϑ as marginal and conditional pdf's of a joint function, except for improving the consistency of the method, may also be useful in a future work where it can be applied for the case of a complete phase matrix.

The probability that an energy packet will follow an after-scattering direction confined within a solid angle interval $\mathrm{d}\Omega$ and inclined at angles φ, ϑ to the direction of incidence is expressed as the ratio of the power scattered into $\mathrm{d}\Omega$ to the power scattered into all directions

$$p(\vartheta,\varphi)\,\mathrm{d}\Omega = \frac{C_\mathrm{s} I_\mathrm{i}(\Omega')\,\mathrm{d}\Omega' \Phi(\vartheta,\varphi)\,\mathrm{d}\Omega}{\int_{4\pi} C_\mathrm{s} I_\mathrm{i}(\Omega')\,\mathrm{d}\Omega' \Phi(\vartheta,\varphi)\,\mathrm{d}\Omega}. \tag{2}$$

In Eq. (2), C_s is the single scattering cross-section, $I_\mathrm{i}(\Omega')$ is the incident intensity within the solid angle $\mathrm{d}\Omega'$, φ and ϑ are the azimuth and polar angles of the scattering direction and $\Phi(\vartheta,\varphi)$ is the phase function. Ω, Ω', φ and ϑ are referred to the relative system of axes carried by the packet. Following the notation of Bohren and Huffman [29], the normalisation of the phase function is such that

$$\int_{4\pi} \Phi(\vartheta,\varphi)\,\mathrm{d}\Omega = \int_0^{2\pi}\int_0^{\pi} \Phi(\vartheta,\varphi)\,\sin\vartheta\,\mathrm{d}\vartheta\,\mathrm{d}\varphi = 1 \tag{3}$$

and thus $p(\vartheta,\varphi)$ reduces to the scattering phase function $\Phi(\vartheta,\varphi)$. The next step is to introduce the cumulative distribution function (cdf), which expresses the joint probability that a scattered energy packet will follow a direction inclined, in reference with the incident, with a polar angle ranging from 0 to ϑ and with an azimuth angle ranging from 0 to φ.

$$R(\vartheta,\varphi) = \int_0^{\varphi}\int_0^{\vartheta} \Phi(\vartheta,\varphi)\,\sin\vartheta\,\mathrm{d}\vartheta\,\mathrm{d}\varphi. \tag{4}$$

The cdf $R(\vartheta,\varphi)$ depends on both the polar and azimuth angles. Therefore it cannot be used directly for sampling one of them. The required functions are derived through the definition of the marginal and conditional cdf's. For the joint cdf (4), two marginal functions can be defined corresponding either to the azimuth or the polar angle. Without loosing generality, only the former marginal cdf and its corresponding conditional will be further examined.

$$R_{\mathrm{m},\varphi} = \int_0^{\varphi}\int_0^{\pi} \Phi(\vartheta,\varphi)\,\sin\vartheta\,\mathrm{d}\vartheta\,\mathrm{d}\varphi, \tag{5}$$

$$R_{\mathrm{c},\vartheta|\varphi} = \frac{\int_0^{\varphi}\int_0^{\vartheta} \Phi(\vartheta,\varphi)\,\sin\vartheta\,\mathrm{d}\vartheta\,\mathrm{d}\varphi}{R_{\mathrm{m},\varphi}}. \tag{6}$$

Eq. (5) expresses the probability that the scattered energy packet will follow a direction having an azimuth angle ranging from 0 to φ independently of the value that the polar angle will take. Eq. (6) expresses the probability that the scattering direction will have a polar angle ϑ under the condition that the azimuth angle has already taken the value φ. The integrals in Eqs. (5) and (6) are numerically evaluated on an angular grid as will be presented in Section 3.1.

Assuming that the fly-ash particles of the bed are spherical, homogeneous, isotropic and non-magnetic, the LMT of elastic scattering can be applied. The applicability of these assumptions is discussed in [1,18–23,30], while it will be further examined in Section 3.1. The azimuthally independent phase function which is derived from the complete phase matrix by ignoring the polarisation state is

$$\Phi_{\mathrm{LMT}}(\vartheta) = \frac{S_{11}(\vartheta)}{\pi x^2 Q_\mathrm{s}}. \tag{7}$$

In Eq. (7), Q_s is the single scattering efficiency, x the size parameter defined as $x = \pi D/\lambda$, where D is the particle diameter, λ the wavelength and $S_{11}(\vartheta) = (|S_1(\vartheta)|^2 + |S_2(\vartheta)|^2)/2$, where S_1 and S_2 are the complex scattering amplitude functions. These depend, except of the scattering angle, on the size parameter and the complex refractive index and are calculated in this study

by the BHMIE program of Bohren and Huffman [29]. Introduction of Eq. (7), turns Eqs. (5) and (6) into

$$R_{\mathrm{m},\varphi} = \frac{\varphi}{2\pi} \tag{8}$$

and

$$R_{\mathrm{c},\vartheta|\varphi} = \frac{1}{x^2 Q_{\mathrm{s}}} \int_0^{\vartheta} \left(|S_1(\vartheta)|^2 + |S_2(\vartheta)|^2 \right) \sin\vartheta \, \mathrm{d}\vartheta. \tag{9}$$

Sampling of the after-scattering angles can be done using the pair of Eqs. (8) and (9). Furthermore, it can easily be shown that $R_{\mathrm{c},\varphi|\vartheta} = R_{\mathrm{m},\varphi}$, $R_{\mathrm{c},\vartheta|\varphi} = R_{\mathrm{m},\vartheta}$ and therefore the choice of either the polar or the azimuth angle to define the marginal and conditional functions leads to the same pair of sampling equations.

The extinction coefficient β_λ appearing in Eq. (1), the scattering albedo ω_λ used to interpret extinction of an energy packet as either absorption or scattering and the phase function $\Phi_{\mathrm{LMT}}(\vartheta)$ appearing in Eq. (7) refer to a monodispersed particle cloud. In the general case where the particles follow a size distribution $f(D)$, they have to be replaced by their averaged equivalents $\overline{\beta}_\lambda$, $\overline{\omega}_\lambda$ and $\overline{\Phi}_{\mathrm{LMT}}(\vartheta)$. Details for the calculation of the first two parameters, as well as the psd-averaged extinction and scattering efficiencies needed in this calculation, can be found in many references, e.g. [20,23]. The third parameter, the psd-averaged phase function is estimated in analogy to Eq. (7) as

$$\overline{\Phi}_{\mathrm{LMT}}(\vartheta) = \frac{\overline{S}_{11}(\vartheta)}{\alpha^2 \overline{C}_{\mathrm{s}}}, \tag{10}$$

where $a = 2\pi/\lambda$, $\overline{C}_{\mathrm{s}} = (\pi/4) D_{20}^2 \overline{Q}_{\mathrm{s}}$, D_{20} is the quadratic mean diameter of a size distribution, $\overline{Q}_{\mathrm{s}}$ the psd-averaged scattering efficiency and $\overline{S}_{11}(\vartheta) = \int_0^\infty S_{11}(\vartheta) f(D) \, \mathrm{d}D$. In the next section, the size distribution $f(D)$ will be given both analytically, in the case where a sensitivity analysis will be performed, and as a discontinuous function as it is measured in [1]. In the latter case, the integral to calculate $\overline{S}_{11}(\vartheta)$ is replaced by a summation over the classes of the particle diameter.

3. Results

In their nephelometric experiment, Boothroyd et al. [1] used a 50 mW He–Ne laser (0.633 μm wavelength) to illuminate fly-ash particles fluidised in a cylindrical bed of 25 mm diameter and 20 mm height. The beam was initially expanded to 24 mm diameter and then clipped to 5 mm in order to provide a "top hat" profile with practically constant intensity. Ash particles were considered to be uniformly dispersed in the bed. In order to account for possible agglomeration, psd's were measured using both a Coulter counter (thereafter Coulter psd) and a Malvern diffraction sizer (thereafter Malvern psd). The extinction of the beam was estimated in the range from 1% to 2%. Comparisons were made in [1] between the measured and the calculated by LMT angular distribution of the scattered intensity using as refractive index for the fly-ash particles the value $n + \mathrm{i}k = 1.5 + \mathrm{i}0.012$.

3.1. Simulation of the nephelometric experiment

The motivation for the numerical simulation of the nephelometric experiment is to validate the models presented in Section 2 and to extract information that will assist laser-based diagnostics applied in dense two-phase flows. The distinction between the solutions obtained by the LMT and the Monte Carlo simulation is hereby recalled; the former states that the wavelets or energy packets by which the laser beam is decomposed may interact with some particle only once, the latter allows the second- or higher-order interaction with other particles. Therefore, even though in Monte Carlo every individual interaction obeys the Lorenz–Mie solution, the "measured" after the numerical experiment scattering pattern may differ from the Mie prediction inasmuch as it is composed of a superposition of single scattering patterns. It should, however, be noted that even in the case that the illuminated cloud is dilute enough to avoid any multiple scattering effects, the simulation of a nephelometric experiment remains an interesting and demanding test case for validating a numerical radiative transfer model.

The bed is subdivided in a small number of 2D cylindrical axisymmetric control volumes. This is done, even though the cloud is homogeneous, to facilitate the ray-tracing algorithm and the application of Eq. (1). The scattering albedo of the ash particles is estimated as the ratio of their scattering over extinction efficiencies, which in turn are defined by averaging over the Malvern psd. No significant differences were observed when the same procedure was applied to the Coulter psd. In this paragraph, the complex refractive index is accepted as suggested in [1].

Since Eq. (9), which is used for sampling the scattering polar angle, cannot be directly inverted, the integral of the right-hand side is calculated for a fine angular mesh. The intervals of this mesh are varying in order to capture the strong forward lobe of the phase function, as well as the weaker but interesting, in some applications, backward lobe. Specifically, in the angular range 0–3° the grid resolution is 0.01°; in the range 3–10°, the angular interval is 0.05°; then in the range 10–20° is increased to 0.1°; further increased to 1° in the range 20–150° and again becomes finer (0.1°) at the backward direction (150–180°). After the numerical integration of the cdf (9) on this grid, the difference between the calculated and the expected value of 1 was found always lower than 10^{-4} and therefore no

normalisation of the cfd was applied. Sampling of the polar angle is made by first assigning a random value to $R_{c,\vartheta|\varphi}$, then finding the angular interval of the mesh where this value falls and then interpolating between the nearest points. Statistics are calculated after repeating the simulation for nine sets of 4×10^9 energy packets.

Results of this simulation are presented in Fig. 2. In this figure, the angular intensities $I(\vartheta)$ calculated by Mie theory have been normalised by the forward intensity $I(0)$, while the Monte Carlo results represent this ratio by the number of energy packets received at angular position ϑ divided by the number of packets received at $\vartheta = 0$. The first observation in Fig. 2 is that there is an excellent agreement between Mie and Monte Carlo results for all the angles except of the range 110–155° where the agreement is fairly good. It will be shown in Section 3.3 that in this region the ratio of the multiple over the total scattering is maximised. However, this is also the region where the numerically simulated received signal is minimised and therefore some influence of statistical fluctuation is also present.

In order to quantify the scattering behaviour of the medium, three indices have been calculated using data from the Monte Carlo simulation. The first one is the sum of energy packets received at all the angular positions after multiple scattering over the total amount of the received scattered packets. This index was found equal to $0.486 \times 10^{-2} \pm 0.1 \times 10^{-4}$, confirming that the experiment of Boothroyd et al. was well designed to avoid any significant effect of multiple scattering. The second index is the ratio of the packets absorbed after single scattering over the totally detected single scatterings. This index is a measure of the extinction of the single scattering signal before it is detected. It was found equal to $0.262 \times 10^{-2} \pm 0.1 \times 10^{-4}$, implying that the detected were almost equal to the actual single scatterings. Furthermore, in the cases where detection of multiple scattering is undesirable, a measure of the ability of the medium to cancel this detection may be useful. This is given by the third index, which is the ratio of the packets absorbed after multiple scattering over the total amount of the detected multiple scattered packets. For the conditions of the examined experiment, the third index was found equal to $0.184 \times 10^{-2} \pm 0.5 \times 10^{-4}$. The calculation of these three indices is an example of the flexibility of the Monte Carlo method and the insight it may provide for the analysis of complex radiative transfer phenomena.

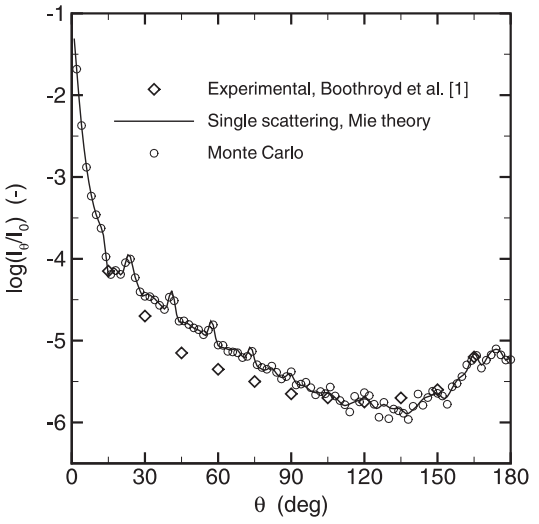

Fig. 2. Angular distributions of the scattered intensities normalised with the intensity at angle $\vartheta = 0$. The solid line, corresponding to the Mie theory, is the scattering pattern calculated considering only single scattering. The cycles correspond to Monte Carlo and they form the scattering pattern after allowing for multiple scattering.

Mie and Monte Carlo results agree with the experimental data in the forward direction (15°) and in the side and backward regions (105–180°). A discrepancy is observable between 15° and 105°. This should be attributed to minor deviations of the actual particles from the ideal sphericity, surface regularity and homogeneity imposed by LMT. However, the important point in Fig. 2 is that the curves remain below the ordinate 10^{-4} for a very wide range of angles ($\vartheta = 15°$ to 180°), while approach in their minimum even the 10^{-6} ordinate. This is an indication that the total scattered intensity is a very small portion of the radiation that propagates within the first 1–2° of the polar angle. Therefore, although detectable and significant for many diagnostic applications, single scattering of fly-ash can hardly realised as an important heat transfer mechanism. That is shown in detail in this paragraph for the wavelength $\lambda = 0.633$ μm, while a relevant discussion for the whole thermal spectrum is cited in [23]. The multiple scattering of fly-ash is investigated in Section 3.3.

3.2. Influence of the optical properties

It is known that the complex refractive index is a key parameter influencing the extinction behaviour of particles. However, uncertainties still do exist about the value of the imaginary part of this index for fly-ash and its dependence on the particle composition. It has been mentioned in Section 1 that Goodwin and Mitchner [20] found a strong wavelength dependence for the imaginary part of this index and generally lower values than what was previously accepted in the literature. In order to evaluate the sensitivity of the results presented in Section 3.1 on the optical properties, the measurements of Goodwin and Mitchner [20], as correlated by Liu and Swithenbank [22], have been used to estimate the complex refractive index for the wavelength of the He–Ne

laser. This index was found to be $m = n + ik = 1.5 + i0.493 \times 10^{-4}$, a value that has significantly lower imaginary part than what was accepted in the previous paragraph. This is an effect of the wavelength dependency of k. It can be seen in Fig. 1 of [20] that the measured k has very low values in the region of the visible wavelengths and only after $\lambda \approx 8$ μm approaches the previously accepted value. The effect of these different optical properties is analysed in the following paragraphs.

The angular distributions of the non-normalised scattered intensities as predicted by LMT for the Malvern psd and for refractive indices according to [1,20] are presented in Fig. 3. It is evident in this figure that the index of Goodwin and Mitchner resulted significantly stronger backward lobe compared to the index of Boothroyd et al. This attribute has been found valid for all the diameters of the Malvern psd. Especially for diameters greater than 50 μm, the combination of the index $m = 1.5 + i0.012$ with the wavelength of the He–Ne laser resulted complete cancelling of the backward lobe. Furthermore, it can be observed in Fig. 3 that the line corresponding to the index reported in [20] lies over the line of [1] for all the angles, except of the forward direction and a rather small region around 120° where they practically coincide. Therefore, it is expected that the asymmetry factor exhibits dissimilarities for the two indices.

In order to quantify this expectation and recover the influence of particle size on the results presented in Fig. 3, radiative properties of particles with diameters from 1 to 200 μm have been calculated for every 0.5 μm for the two indices. The calculated asymmetry factor is presented in Fig. 4 for diameters up to 30 μm. For larger diameters, this parameter was found practically constant around 0.82 and 0.95 for the optical properties according to [1,20], respectively. Although this is a significant difference, it can be seen in Fig. 5 that even more distinct are the albedos of these two kinds of particles. For $k = 0.49 \times 10^{-4}$, ω is between 1 and 0.98 for the

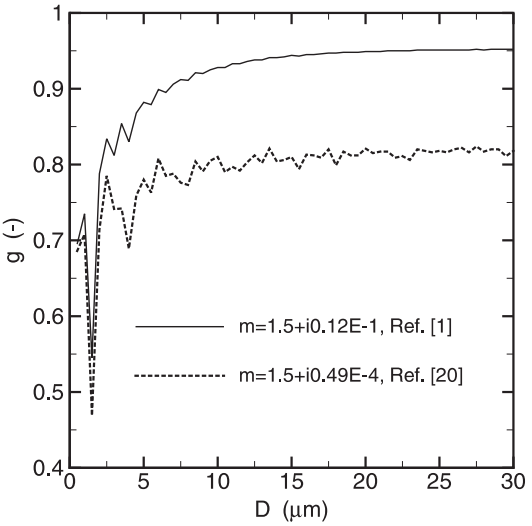

Fig. 4. Comparison of the asymmetry parameter for complex refractive indices according to Boothroyd et al. [1] and Goodwin and Mitchner [20] for a range of fly-ash particle diameters and $\lambda = 0.633$ μm.

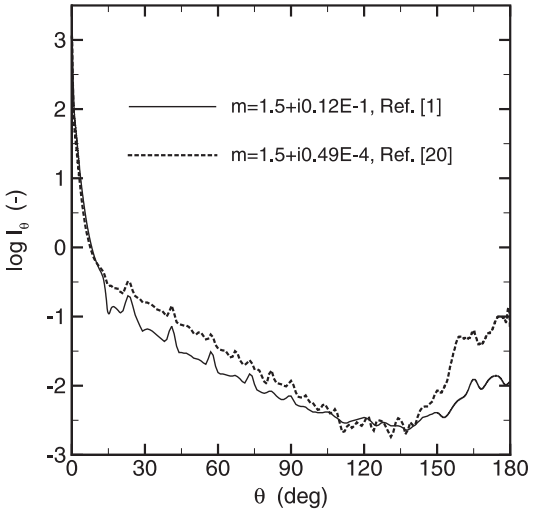

Fig. 3. The influence of the fly-ash optical properties on the angular distribution of the scattered intensities. Calculations correspond to single scattering (Mie theory) and the wavelength of the He–Ne laser.

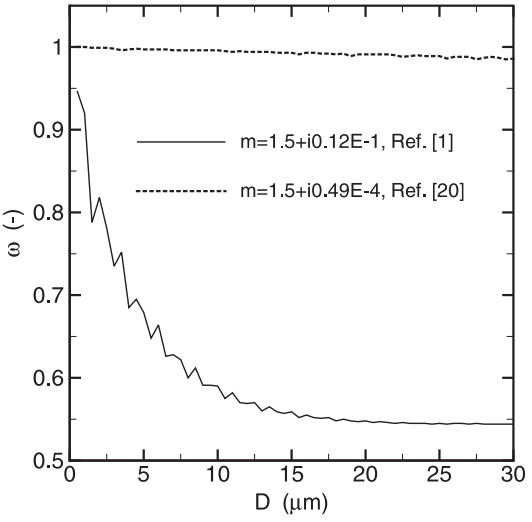

Fig. 5. Comparison of the scattering albedos for two different refractive indices of fly-ash in the range of 0–30 μm particle diameters and 0.633 μm wavelength.

diameter range 0–30 μm, while after this range it remains practically constant up to 200 μm. For $k = 0.12 \times 10^{-1}$, the albedo has the value 0.95 for very small particles, sharply declines to 0.55 for diameters around 20 μm and retains this value up to 200 μm. The differences in the extinction efficiency, shown in Fig. 6, are minor with the fly-ash of [20] exhibiting a more oscillating behaviour around the values calculated for the fly-ash of [1]. In summary, clouds made of fly-ash particles with optical properties according to [1,20] will extinguish rather equally the incident laser beam, with the former cloud having the tendency of more forward scattering. However, in the latter cloud almost every extinction event will be scattering since the albedo is characteristic of a conservatively scattering medium, and that independently of the particle diameter. Furthermore, it can be seen in Figs. 4–6 that the variation of the examined properties in respect of the particle diameter is smooth enough to be adequately represented by a psd-averaged property.

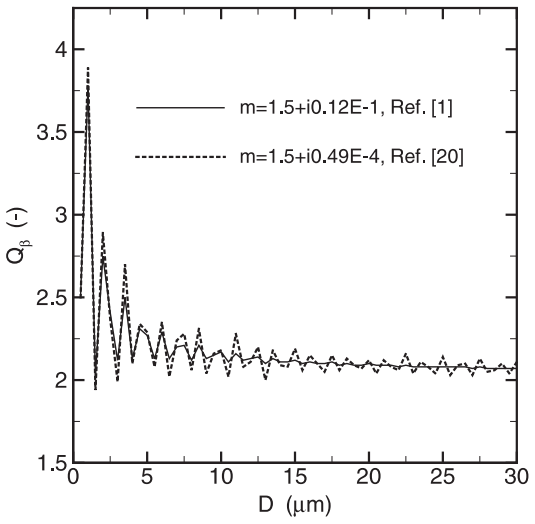

Fig. 6. Extinction efficiencies depending on the refractive index of fly-ash particles for the 0–30 μm diameter range and 0.633 μm wavelength.

3.3. Influence of multiple scattering

The concentration of the ash particles in the experiment examined in Section 3.1 was dilute enough to practically avoid multiple scattering. However, this phenomenon plays an important role in many practical systems. In order to gain a better insight, a numerical experiment is performed concerning the extinction of the same laser beam by a suspension of particles with considerably higher optical depth. The relevant data are summarised in Table 1. Particles are assumed to follow the refractive index of [20] and a gamma size distribution [17]

$$f(D) = \frac{t b^{(q+1)/t} D^q \mathrm{e}^{-qD/D_\mathrm{p}}}{\Gamma((q+1)/t)}. \tag{11}$$

In Eq. (11), $\Gamma(x)$ denotes the gamma function of the variable x, $b = (q/t)D_\mathrm{p}^{-t}$, D_p is the most probable (peak) diameter and q, t are adjustable parameters. The psd-averaged asymmetry factor, scattering albedo and extinction efficiency are found equal to 0.79, 0.99 and 2.2, respectively. The optical depth of the bed is equal to 0.625 and therefore the extinction of the laser beam is estimated in the order of 46.5%. This is considerably higher than the case of 1–2% extinction examined in Section 3.1.

The combination of the increased optical depth and the very high albedo implies that the energy packets may undergo a high percentage of multiple scattering before reaching the virtual detector. To quantify that, seven sets of 10^8 packets were traced and the qualitative indices of Section 3.1 were calculated. The ratio of the multiple scattered packets over the totally detected was found equal to $0.2731 \pm 0.1 \times 10^{-3}$. The percentages of the packets absorbed after single and multiple scattering were found insignificant. That was expected due to the very high albedo which favours scattering in place of absorption events.

The angular distribution of the intensities detected after single and multiple scattering, together with the distribution of the total detected energy packets is plotted in Fig. 7. All the values depicted in this figure have been normalised by the amount of energy packets received at $\vartheta = 0$. It can be observed that the line

Table 1
Data used for the case of increased optical depth

Input data			Calculated data		
Size distribution	D_p	6.0 (μm)	Size distribution	D_{20}	7.3 (μm)
	q	2 (dimensionless)		D_{30}	7.9 (μm)
	t	2 (dimensionless)		D_{32}	9.0 (μm)
Density	ρ	2.6×10^3 (kg/m^3)	Extinction efficiency	$\bar{Q}_\beta$	2.2 (dimensionless)
Concentration	c	1.8×10^{-2} (kg/m^3)	Asymmetry factor	$\bar{g}$	0.79 (dimensionless)
Refractive index	$n + \mathrm{i}k$	$1.5 + \mathrm{i}0.493 \times 10^{-4}$	Albedo	$\bar{\omega}$	0.99 (dimensionless)

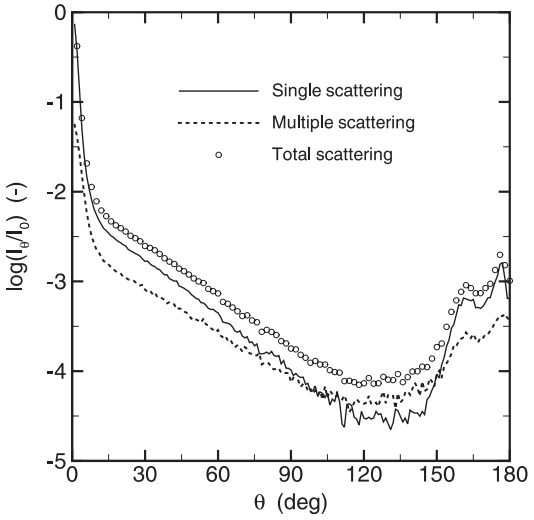

Fig. 7. Angular distributions of the single, multiple and total scattered intensities for the case of increased optical depth.

corresponding to total scattering has a wider forward lobe compared with the single scattering line, while it lies over this line for the whole angular range. A smoothing effect due to multiple scattering is apparent in Fig. 7, implying that the medium tends to be sensed by the virtual detector as an increasingly isotropic scatterer as the proportion of multiple scattering also increases.

Another observation that can be made in Fig. 7 is that the line of multiple scattering lies over the line of single scattering in the region between 105° and 150°. This observation implies that in this angular interval the majority of the received packets originate from multiple scattering. In order to obtain a clearer picture, the ratio of the multiple over the total received intensity is plotted in Fig. 8. The minimum values of this ratio occur in the first 6°. However, it should be noted that this angular region is not easily handled in laser measurements due to the interference of the collecting optics and the transmitted beam. Instead, the small angular interval between 160° and 170° in the backward direction would be preferable for laser measurements as it offers relatively clear single scattering signal.

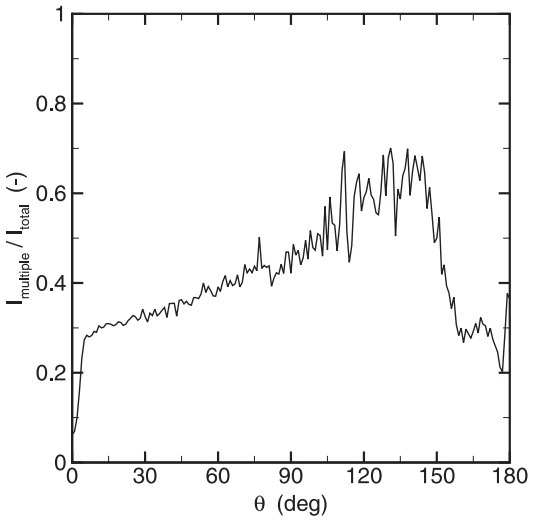

Fig. 8. Angular distribution of the multiple over the total scattering ratio for the case of increased optical depth.

4. Conclusions

In this paper, a Monte Carlo method was applied to simulate the extinction of a laser beam irradiating a cloud of fly-ash particles. The objective was threefold: first, to validate the method and the accompanying models against a simple well-defined experiment; second, to demonstrate how this method could be potentially used to assist laser-based diagnostics, and third, to derive any firm conclusion about the effect of fly-ash on radiative heat transfer in coal furnaces.

It was shown that the combination of the Monte Carlo algorithm and the exact Lorenz–Mie phase function correctly recovered the angular distribution of the scattered intensity at distant detection points. This is a simple numerical experiment intended for code validation of ray-tracing algorithms in scattering media. Furthermore, a decisive parameter for the application of laser diagnostics in dense two-phase flows is the penetration length for which the scattered light can be meaningfully recovered. It was shown how the developed method helped to identify an angular interval where, if these measurements were applied for fly-ash, the detection of multiple scattering would have been minimised.

All the computations and analyses of this study were monochromatic, restricted on the wavelength of the He–Ne laser. However, two observations that can be extended to the whole thermal spectrum have been made: first, fly-ash scattering is so anisotropic in the forward direction that neglecting of scattering is a reasonable approximation in applications where only single scattering is favoured, and second, multiple scattering tends to smooth the sharp forward single scattering pattern. The latter observation has been made for the test case of increased optical depth although the dimensions of the examined bed were considerably small. Therefore, in modelling of large-scale furnaces where the control volumes, due to computing restrictions, have multiples of the examined dimensions, an even stronger smoothing effect of multiple scattering is expected. In this case, the introduction of an apparent phase function calculated as a modification, due to multiple scattering, of the exact Lorenz–Mie phase function, seems to be the feasible future modelling approach.

Acknowledgements

This work has been partially financed by the Commission of the European Communities through the TMR network "Fundamental improvements in radiative heat transfer – RADIARE" (CT-98-224). The first author would like to acknowledge the useful discussions he had with Prof. M. Pinar Mengüç and Prof. Rolf Hernberg.

References

[1] S.A. Boothroyd, A.R. Jones, K.W. Nicholson, R. Wood, Light scattering by fly ash and the applicability of Mie theory, Combust. Flame 69 (1987) 235–241.
[2] S.S. Penner, C.P. Wang, M.Y. Bahadori, Laser diagnostics applied to combustion systems, in: Twentieth Symposium (International) on Combustion, The Combustion Institute, Pittsburgh, PA, 1984, pp. 1149–1176.
[3] D. Stepowski, Laser measurements of scalars in turbulent diffusion flames, Prog. Energy Combust. Sci. 18 (1992) 463–491.
[4] S. Lederman, The use of laser Raman diagnostics in flow fields and combustion, Prog. Energy Combust. Sci. 3 (1974) 1–34.
[5] S. Subramaniam, M.P. Mengüç, Solution of the inverse radiation problem for inhomogeneous and anisotropically scattering media using a Monte Carlo technique, Int. J. Heat Mass Transfer 34 (1991) 253–266.
[6] F. Durst, A. Melling, J.H. Whitelaw, Principles and Practice of Laser Doppler Anemometry, second ed., Academic Press, San Diego, 1981.
[7] R. Siegel, J.R. Howell, Thermal Radiation Heat Transfer, third ed., Taylor and Francis, Washington, DC, 1992.
[8] J.R. Howell, The Monte Carlo method in radiative heat transfer, J. Heat Transfer 120 (1998) 547–560.
[9] F.C. Lockwood, N.G. Shah, A new radiation solution method for incorporation in general combustion procedures, in: Proceedings of the Eighteenth Symposium (International) on Combustion, The Combustion Institute, Pittsburgh, PA, 1981, pp. 1405–1414.
[10] P.J. Coelho, M.G. Carvalho, A conservative formulation of the discrete transfer method, J. Heat Transfer 119 (1997) 118–128.
[11] L. Zhang, A. Soufiani, J. Taine, Spectral correlated and non-correlated radiative transfer in a finite axisymmetric system containing an absorbing and emitting real gas–particle mixture, Int. J. Heat Mass Transfer 31 (1988) 2261–2272.
[12] J.G. Marakis, Application of narrow and wide band models for radiative transfer in planar media, Int. J. Heat Mass Transfer 44 (2001) 131–142.
[13] F. Liu, Numerical solutions of three-dimensional non-grey gas radiative transfer using the statistical narrow band model, J. Heat Transfer 121 (1999) 200–203.
[14] C. Sasse, Development of an experimental system for optical characterization of large arbitrary shaped particles, Rev. Sci. Instrum. 64 (1993) 864–869.
[15] B.M. Agarwal, M.P. Mengüç, Forward and inverse analysis of single and multiple scattering of collimated radiation in an axisymmetric system, Int. J. Heat Mass Transfer 34 (1991) 633–647.
[16] R. Viskanta, M.P. Mengüç, Radiation heat transfer in combustion systems, Prog. Energy Combust. Sci. 13 (1987) 97–160.
[17] A.G. Blokh, Heat Transfer in Steam Boiler Furnaces, Hemisphere, Washington, DC, 1988.
[18] R.P. Gupta, T.F. Wall, J.S. Truelove, Radiative scatter by fly ash in pulverized coal-fired furnaces: application of the Monte Carlo method to anisotropic scattering, Int. J. Heat Mass Transfer 26 (1983) 1649–1660.
[19] R.P. Gupta, T.F. Wall, The optical properties of fly ash in coal fired furnaces, Combust. Flame 61 (1985) 145–151.
[20] D.G. Goodwin, M. Mitchner, Flyash radiative properties and effects on radiative heat transfer in coal-fired systems, Int. J. Heat Mass Transfer 32 (1989) 627–638.
[21] K.H. Im, R.K. Ahluwalia, Radiation of coal combustion products, Int. J. Heat Mass Transfer 36 (1993) 293–302.
[22] F. Liu, J. Swithenbank, The effects of particle size distribution and refractive index of fly-ash radiative properties using a simplified approach, Int. J. Heat Mass Transfer 36 (1993) 1905–1912.
[23] J.G. Marakis, C. Papapavlou, E. Kakaras, A parametric study of radiative heat transfer in pulverised coal furnaces, Int. J. Heat Mass Transfer 43 (2000) 2961–2971.
[24] M.Q. Brewster, Thermal Radiative Transfer and Properties, Wiley, New York, 1992.
[25] M.F. Modest, Radiative Heat Transfer, McGraw-Hill, New York, 1993.
[26] A. Haji-Sheikh, Monte Carlo methods, in: W.J. Minkowycz, E.M. Sparrow, G.E. Schneider, R.H. Pletcher (Eds.), Handbook of Numerical Heat Transfer, Wiley, New York, 1988, pp. 673–722.
[27] W.J. Yang, H. Tanigushi, K. Kudo, Radiative heat transfer by the Monte Carlo method, in: J.P. Hartnett, T. Irvine (Eds.), Adv. Heat Transfer, vol. 27, Academic Press, San Diego, 1995, pp. 1–215.
[28] J.T. Farmer, J.R. Howell, Monte Carlo strategies for radiative transfer in participating media, in: J.P. Hartnett, T. Irvine (Eds.), Adv. Heat Transfer, vol. 31, Academic Press, San Diego, 1998, pp. 1–97.
[29] C.F. Bohren, D.R. Huffman, Absorption and Scattering of Light by Small Particles, Wiley, New York, 1983.
[30] G. Gouesbet, G. Grehan, B. Maheu, Single scattering characteristics of volume elements in coal clouds, Appl. Opt. 22 (1983) 2038–2050.